Preprint
UCRL-JC-135621

Ultrasonic Velocities in Unconsolidated Sand/Clay Mixtures at Low Pressures

C.M. Aracne-Ruddle, B.P. Bonner, C.N. Trombino, E.D. Hardy, P.A. Berge, C.O. Boro, D. Wildenschild, C.D. Rowe and D.J. Hart

This article was submitted to
American Geophysical Union Fall Meeting
San Francisco, CA
December 13-17, 1999

U.S. Department of Energy

Lawrence
Livermore
National
Laboratory

October 15, 1999

Ultrasonic Velocities in Unconsolidated Sand/Clay Mixtures at Low Pressures

C. M. Aracne-Ruddle, B. P. Bonner, C. N. Trombino, E. D. Hardy, P. A. Berge, C. O. Boro, D. Wildenschild, C. D. Rowe, and D. J. Hart

Abstract

Effective seismic interrogation of the near subsurface requires that measured parameters, such as compressional and shear velocities and attenuation, be related to important soil properties. Porosity, composition (clay content), fluid content and type are of particular interest. The ultrasonic (100-500 kHz) pulse transmission technique was used to collect data for highly attenuating materials appropriate to the vadose zone. Up to several meters of overburden were simulated by applying low uniaxial stress of 0 to about 0.1 MPa to the sample. The approach was to make baseline measurements for pure quartz sand, because the elastic properties are relatively well known except at the lowest pressures. Clay was added to modify the sample microstructure and ultrasonic measurements were made to characterize the effect of the admixed second phase. Samples were fabricated from Ottawa sand mixed with a swelling clay (Wyoming bentonite). The amount of clay added was 1 to 40% by mass. Compressional (P) velocities are low (228 – 483 m/s), comparable to the sound velocity in air. Shear (S) velocities are about half of the compressional velocity (120 – 298 m/s), but show different sensitivity to microstructure. Adding clay increases the shear amplitude dramatically with respect to P, and also changes the sensitivity of the velocities to load. These experiments demonstrate that P and S velocities are sensitive to the amount of clay added, even at low concentrations. Other properties of the transmitted signals including the ratio of S and P amplitudes, velocity gradient with depth, and the frequency content of transmitted pulses, provide additional information about the clay content. Direct observation of sand-clay microstructure indicated that the clay particles electrostatically cling to the sand grains but do not form a coating. Instead, in the dry mixture clay particles tended to bridge the gaps between grains, influencing how stresses were carried across grain contacts. Because of this tendency to bridge the gaps, small amounts of clay can have large effects on the wave propagation.

Introduction

Effective in-situ remediation requires knowledge of subsurface porosity, permeability, and fluid saturation. Only after the site has been characterized can the cleanup begin. Using geophysical techniques to image the subsurface is much cheaper and less invasive than drilling many sampling wells. There is a shortage of data for unconsolidated materials for loading conditions typical of near subsurface conditions. This laboratory effort is part of a larger program to combine seismic and electrical characterization methods. This method is described in detail at (www-ep.es.llnl.gov/www-ep/esd/expgeoph/Berge/EMSP/intro.html). Electrical methods have usually been used for environmental applications, but recent advances in high-resolution reflection (Steeples, 1998) and crosswell seismic methods (e.g., Harris et al., 1995) suggest that combined electrical and seismic techniques could be a powerful tool for imaging the shallow subsurface.

Surface and cross-hole seismic methods are now a standard tool for site investigations. Seismic surveying and imaging are being used to address a broad variety of engineering, environmental and ground water problems. Typical

applications include locating perched water Tables, tracking fluid movement in the subsurface and delineating landfills. Measured seismic properties have been available for many years and are used in a wide variety of applications including geotechnical (Whitman, 1966), sediment acoustics (Hamilton and Bachman, 1982) as well as basic studies of porous media (Wyllie et al., 1958). Unfortunately, relating the measured seismic attributes to material properties and composition is difficult for environmental problems. The difficulty is that there are gaps in measurements for appropriate media under controlled laboratory conditions.

For example, measurements at low pressure representative of the first 10 meters depth are not available because of extremely high attenuation. Measurements are sparse for partially saturated soils, again because of high attenuation. Shear wave measurements in general are more difficult because the arrival is obscured by earlier compressional energy. Although it is widely appreciated that clay content of a mineral soil is an important factor in controlling the seismic attributes, the coupled mechanical and chemical effects expected for clays have not been investigated in detail. The purpose of the work described in this paper is to begin addressing some of these shortcomings in the literature and to develop more effective methods for extracting soil properties, such as water content and soil composition, from field seismic data.

Background

Site characterization is an important step towards in-situ remediation. Several methods have been used to examine the physical properties of soil in the near subsurface. One important method is seismic interrogation, which involves measuring the velocities of elastic waves that travel through the subsurface. Effective seismic interrogation requires that measured parameters be related to soil properties. Laboratory experiments that measure elastic wave velocities in manufactured soils can provide field researchers with methods for interpreting field-collected data.

Since the elastic properties of pure quartz sand are well known (Domenico, 1976) except at the lowest pressures, pure quartz sand is often used to make reference measurements. The microstructure of the sample is altered with controlled “impurities” such as clay, and ultrasonic measurements are then made in the laboratory to characterize the associated effects.

In laboratory samples, it has been found that small amounts of swelling clay dramatically change the way seismic energy propagates through unconsolidated soils (Bonner et al., 1997). Seismic field data are therefore disproportionately affected by the presence of swelling clay. Clay blocks fluid flow, and to a large degree controls how fluids circulate as contaminants spread or are removed by remediation.

Soil composition (i.e., clay content) is only one factor that influences contaminant transport in the near subsurface. Other parameters such as porosity, permeability, and fluid saturation are important to site characterization. Electrical methods have been used to quantify these parameters, and studies (Harris et al., 1995, Berge et al.,

1998) suggest that these methods could be combined with seismic information about compressional and shear velocities to image the shallow subsurface.

Theoretical Background

The two types of elastic waves that are important to seismic investigation are the compressional, or primary (P) waves and the shear, or secondary (S) waves. Both of these waves fall under the category of body waves, or waves that travel through the interior of a rock body. P-waves travel in any direction where compression is opposed, inducing longitudinal oscillatory particle motions similar to simple harmonic vibrations. Secondary or shear (S) waves propagate more slowly than P-waves and have particle motion perpendicular to the direction of wave propagation. S-waves can be byproducts of P-waves, occurring when P-waves impinge on a free boundary and cause displacement. S-waves only travel in material that resists changes in shape, so they do not travel in fluids. A complete description of the theory of wave propagation is given by Aki and Richards (1980).

Elastic waves with seismic frequencies (about .01 Hz to 10 kHz) are called seismic waves. Sound waves are P-waves at frequencies that the human ear can detect (about 20 Hz to 20 kHz). Elastic waves with high frequencies (> 20 kHz) are called ultrasonic waves.

The velocity of the propagating wave is determined by the elastic properties of the medium, as given in the following equations (Lama and Vutukuri, 1978):

$$v_P = \left[\frac{E(1-\nu)}{\rho(1+\nu)(1-2\nu)}\right]^{\frac{1}{2}} = \left[\frac{K+\frac{4}{3}G}{\rho}\right]^{\frac{1}{2}} \qquad (Eq.\ 1)$$

$$v_S = \left[\frac{G}{\rho}\right]^{\frac{1}{2}} = \left[\frac{E}{2\rho(1+\nu)}\right]^{\frac{1}{2}} \qquad (Eq.\ 2)$$

where

v_P = velocity of compressional waves, m/s
v_S = velocity of shear waves, m/s
E = dynamic modulus of elasticity (Young's modulus), Pa
K = dynamic bulk modulus (inverse of compressibility), Pa
G = dynamic modulus of rigidity, Pa
ν = Poisson's ratio, and
ρ = density, kg/m^3.

In this laboratory experiment, ultrasonic wave velocities for P- and S- waves were determined from measured wave arrival times and the known lengths of the samples:

$$v = \frac{10^4 l}{t_{arr} - t_0} \qquad (Eq.\ 3)$$

where

v = velocity (of compressional or shear waves), m/s
10^4 = factor converting cm/μs to m/s
l = distance traveled by wave, measured to be 1.770 ±0.005 in (4.496 ±0.013 cm), and
t_{arr} = observed arrival time of wave, μs
t_0 = system correction time (t_0 established by aluminum calibration experiments), μs.

The aluminum calibration experiments involved substituting pure aluminum samples for the regular samples to determine the total lag time introduced by cables and connections in the sample setup. The aluminum samples were different length sections cut from a single aluminum bar. The arrival times were measured (see **Experimental Setup and Procedure** section) and plotted against length. The y-intercept given by a linear fit is the time adjustment. The compressional time adjustment (t_{P0}) was determined to be 1 μs, and the shear time adjustment (t_{S0}) was 3 μs.

The total volume of the sample was measured by filling an empty sample assembly with deionized water, extracting the water with a syringe, then measuring the volume of the water in a graduated cylinder (knowing that 1 ml = 1 cm^3). The density of the pure sand sample was determined to be 1700 kg/m^3 from the volume of the cylinder, 78 cm^3 ± 5%, the mass of sand, 131.97 grams and the equation relating the two:

$$\rho = 1000 \frac{m}{V} \qquad (Eq.\ 4)$$

where

1000 is the factor converting r to kg/m^3,
m = mass, g
V = volume, cm^3.

Densities of the other samples are discussed later in this paper in the results section and in the appendix.

The dynamic modulus of rigidity (G) was found by solving the shear velocity equation (Equation 2) in terms of experimentally determined values. The dynamic bulk modulus (K) was then calculated by solving the compressional velocity equation (Equation 1) in terms of experimentally determined values and G. Poisson's ratio was found by simultaneously solving the two velocity equations, yielding

$$\nu = \frac{\frac{2G}{\rho} - v_P^{\,2}}{\frac{2G}{\rho} - 2v_P^{\,2}} = \frac{1 - 2\left(\frac{v_S}{v_P}\right)^2}{2 - 2\left(\frac{v_S}{v_P}\right)^2}. \qquad (Eq.\ 6)$$

The numerical value of Poisson's ratio can then be substituted into the equation relating the elastic moduli to find the dynamic modulus of elasticity (E):

$$E = 2G(1+\nu). \qquad (Eq.\ 7)$$

Representative elastic moduli were found by substituting the experimentally determined velocities and densities into the previous relationships. The values for E, G, and K were divided by a factor of 10^6 to yield results in units of MPa, as shown in the appendix.

Experimental Setup and Procedure

Sample Preparation

Every sample used pure quartz (Ottawa) sand. This sand comes from a quarry near the city of Ottawa, Illinois and is Middle Ordovician in age. The sand is composed entirely of quartz grains (Domenico, 1976). The grain sizes of the tested sand are between 74 and 420 microns, and the median grain diameter is 273 microns (Aracne-Ruddle et al., 1998). The clay used in our samples was Wyoming bentonite, a Na-montmorillonite.

The sand-clay mixtures used in each sample were combined and weighed separately, and the weight percentages are calculated precisely. This experiment used samples with sand-clay layer weight ratios of 99:1, 97:3, 90:10, 80:20, 70:30, and 60:40 in addition to the (control) 100% sand sample (Table 1).

Every dry sample was prepared following the same procedure. First, the sample assembly (acrylic shell, latex caps, and rubber o-rings) is weighed empty. After the sample assembly mass has been recorded, the assembly is filled to approximately 1/3 of its volume by a portion of the sand-clay mixture. The sand-clay mixture is

packed by a hand-held brass weight that fits snugly inside the acrylic shell. The combination of assembly and sand-clay mixture is weighed, and the mass is recorded. Next, the assembly is filled to approximately 2/3 of its capacity by adding a layer of pure sand, and the contents of the assembly are packed again. The assembly and its contents are re-weighed, and the mass is recorded. Finally, the assembly is filled to capacity with a second layer of the sand-clay mixture, packed, and weighed. The final weight is recorded. The true masses of the assembly and each layer of material are used to calculate approximate layer and total densities. The middle layer prevented the expanding clay from clogging the frits in the fluid intake ports when the sample was saturated. See Tables 1 and 4 and the appendix for densities of the sand/clay layers.

Measurements were made for the dry case only for all of the samples except the 3% clay/sand sample. For that sample we also made measurements with filtered deionized water (DI) and a 0.1 N $CaCl_2$ solution. We used 0.1 N $CaCl_2$ for the brine because the Na+ and other ions in the Na-montmorillonite would be replaced by Ca++ ions, forming a more uniform composition for the clay so that our experiments using simple materials (Ottawa sand and Ca-montmorillonite) would be repeatable. Finally, we replaced the brine with DI water and repeated our measurements to find how the swelling of the clay would affect the measurements. (Note that the "dry" clay is not completely dry and may be affected by the room humidity. Future experiments under controlled humidity conditions will address this question.) Velocities for the dry case for all samples and the saturated 3% clay/sand mixture will be presented in the results section and in the appendix.

Ultrasonics

The experimental setup was based on the method of ultrasonic pulse transmission (Sears and Bonner, 1981) and is shown in schematic form in figure 1. Bonner et al. (1997) and Trombino (1998) previously used this apparatus.

Each sample was a packed mix of dry (room-temperature and humidity) Ottawa sand and sodium montmorillonite, a swelling smectite in a plastic sleeve designed to ensure that the signal was transferred through the soil mixture, rather than the sleeve (Bonner et al., 1999). The length of the sleeve was 4.496 ± 0.013 cm. The sample assembly was closed with latex membranes held in place by rubber O-rings. Latex was chosen to contain the soil mixture because it elastically deforms with the soil when pressure is applied and it has a minimal impact on the signal transmission.

The sample sleeve was equipped with fluid inlet ports sealed with permeable stainless steel frits. These ports could be connected to a gas or liquid source. Before liquid saturation, the pore space was repeatedly flushed with CO_2 , which is much more soluble in aqueous solutions than air. This makes complete saturation easier to achieve.

For each measurement, a sample was placed between two heavily damped 500 kHz transducers polarized for transverse shear (made by Panametrics) for elastic wave measurements, and was locked in place by adjusting the separation between the

transducers to a minimum. The transducers produced sufficient compressional energy to identify both P- and S- wave arrivals. End-load pressures between 0 and 15.6 psi (0 to 0.11 MPa), simulating up to several meters of overburden were applied to the sample through air-driven, pneumatic pistons (manufactured by Bimba) that pushed on the backs of the transducers. Although some small pressure (estimated to be less than 1 psi) was applied in the locking process, this was necessary for coupling.

The end-load pressures were slowly applied in increments of 1.56 psi up to 15.6 psi, inducing static internal stress throughout the loading and unloading of the sample. To ensure consistent loading, house air (at 100 psi) was sent through a miniature compressed air filter (made by C. A. Norgren Co.) and a (Coilhouse Pneumatics) miniature regulator before it reached the pneumatic pistons.

A pulse generator (Figure 1) sent 500 positive volts to activate the transmitting piezoelectric transducer (Transducer #1). The resultant ultrasonic wave produced by Transducer #1 traveled through the sample to the receiving transducer (Transducer #2). This ultrasonic wave was the dynamic stress that was used to test the sample. Transducer #2 converted the ultrasonic wave into electrical form, and the final signal was sent through a 40 to 60db signal preamplifier (a Panametrics preamp with a band pass of 20 kHz to 2 MHz) to a LeCroy 9400 Dual 125 MHz digital oscilloscope (Oscilloscope #1). Oscilloscope #1 plotted the excitation signal sent to Transducer #1 (Channel 1) and the signal received by Transducer #2 (Channel 2) as functions of time. The pulse generator provided timing synchronization to both oscilloscopes. The Channel 1 display established the signal starting time. The Channel 2 information was simultaneously sent to a LeCroy 9430 10 bit 150 MHz digital oscilloscope (Oscilloscope #2). Oscilloscope #1 and Oscilloscope #2 produced identical functions of the Channel 2 data by averaging 1000 sequential repetitive signals to improve the signal-to-noise ratio.

After the pre-amp and oscilloscope settings were adjusted to prevent clipping, the arrival times of the compressional (P) and shear (S) waves were determined through observation of the Channel 2 display and recorded. Oscilloscope #2 digitized the collected data and sent them to an attached Macintosh computer (MAC #1) through a transfer program written using National Instruments LabView software. MAC #1 was networked to another Macintosh computer (MAC #2), where the data were stored for data reduction and signal processing using the Synergy Software program KaleidaGraph. A LabView program (currently being written) will filter the data, determine the frequency content, and automate the arrival time selection. Arrival times and velocities are presented in the Results section.

Ultrasonic Results

The arrival times for all of the samples are shown in Table 2. The pressures in the table are reported in gauge units and psi (1MPa=14.5 psi). The letter designations in the arrival time columns correspond to distinctive features in the waveform.

Sketches in the laboratory notebook display these features. The error is the approximate uncertainty in the picked time. The final columns provide information about saved waveforms and notes.

Velocities determined from the adjusted arrival times are presented in Table 3 together with pressures. This table also includes the adjusted arrival time corrected for the system delay. Pressures are provided in MPa as well as psi. In most cases the "a" picks in Table 2 were used in equation 3 to compute the velocities in Table 3 as well as the velocities in Figures 5 and 6. The uncertainties in the velocities are a function of the signal quality that changes rapidly with loading stress. The travel time uncertainties given in Table 2 typically translate into velocity uncertainties of about 10% at the lowest pressures, decreasing to about 3% at the highest pressures for both P and S waves.

The Table 3 velocities are approximate velocities for the sand/clay mixtures. The procedures followed for adjusting the sand/clay velocities to remove the effects of the sand layer in the middle of the sample are described in the appendix. The corrected velocities are presented in Table 5 and Figures 10 and 11.

Representative waveforms for Ottawa sand and sand with 3% clay are presented in Figure 2 to give a general idea of the quality of the data and to demonstrate the dramatic effects of composition and microstructure. The upper trace shows a waveform for dry sand with the shear pulse peaking at approximately 240×10^{-6} s. The amplitude ratio of shear to compressional pulses is ~1.7. When 3% clay is added, the shear pulse grows in relative amplitude and sharpens indicating higher frequency content. The S to P amplitude ratio is ~4.5. Both observations are consistent with a relative decrease in shear attenuation. The third waveform shows the effect of DI water saturation. The changes caused by saturation relative to a dry sample are dramatic. The compressional velocity increased by a factor of 4 to 5 to approximate the velocity for water, 1.5 km/s. The compressional wave dwarfs the shear arrival, which is difficult to determine in the saturated sample. When the sample is saturated, the acoustic response is similar to that of a mechanical suspension.

We made preliminary tests of the effects of fluid chemistry using the 3% clay/sand sample (Bonner et al., 1997). Figures showing these results can be found on the web page at www-ep.es.llnl.gov/www-ep/esd/expgeoph/Berge/EMSP/agu97poster.html and will not be shown in this paper.

First we made measurements using the brine-saturated 3% clay/sand mixture, and then we replaced the pore fluid with DI water and observed changes in the arrivals. To monitor the flushing process, we measured the electrical conductivity of the effluent as a function of time. The conductivity data are shown in Figure 3a. The conductivity drops 3 orders of magnitude in the first 20 minutes of flushing. Much of the rapid change probably occurs as the brine in the high permeability sand layer is replaced by DI water. Initially the travel time increases as the DI water replaces brine in the permeable sand layer between the fluid ports (Figure 3b). This is expected because the compressional velocity of DI water is lower than the velocity

in brine. Then after approximately 15 to 20 minutes, the travel time starts to decrease as the DI water diffuses into the sand/clay layers in the sample. After about 30 minutes, the travel time no longer decreases significantly. It reaches a stable value where it remains for several hours as the flushing continues.

We were unable to completely replace the brine with DI water using this saturation technique because the swelling of the clay decreased the permeability of the sample. Next we decided to drain the sample completely and then resaturate it with the DI water. We evacuated the 3% clay/sand mixture to drain the pore fluid, and measured arrivals in the sample before resaturating it. Although the sample was drained, it was not completely dry because of water held in the clay. We noted a small amplitude and high frequency content for P. Vp was much faster than in the dry case. The shear arrival was very weak (if present) and appeared at later times than in the plot for the dry 3% clay/sand sample.

We flushed the drained 3% clay/sand mixture with CO_2 and then resaturated it with DI water as the pore fluid. Then we measured arrivals in the saturated sample. We measured compressional wave arrival times as a function of uniaxial pressure, for both the drained case and the DI water-saturated case. High grain contact stiffness was preserved by the residual water absorbed by the swelling clay in the drained sample, producing a weak but fast compressional arrival. After two hours of flushing with DI water, the compressional wave arrival time was approximately the same as in the brine-saturated case and the drained case. The amplitude was about 4 times that seen in the drained case but much smaller than the amplitude for the brine-saturated case. The amplitude grew as we continued flushing with DI water. The amplitude after 2 hours of flushing was only about 5% of the final amplitude that was attained after several additional hours of flushing with DI water. Further work is necessary to understand these fluid effects.

Figure 4 shows two superimposed waveforms that illustrate the effect of time on wave propagation for the dry 10% sand-clay mixture. Load was not applied in either case. After four days, amplitudes for both the P and S waves increased. We speculate that adhesion by the clay increases as water vapor present in the ambient air diffuses into the montmorillonite. An alternative explanation would be creep of clay separating sand grains, improving sand-to-sand contacts. This is unlikely because the sample was not loaded and internal stresses should be low. The increase in velocity was almost undetectable.

Velocities for sand-clay mixtures are plotted in Figure 5 to illustrate that velocities are low and increase rapidly with small static loads. For the pure sand sample, the compressional velocity changes with load even at the lowest loads. When clay is added, the increase with pressure is delayed until the stress level reaches approximately 8 psi (0.06 MPa), roughly equivalent to a subsurface depth of 3 meters. The shear velocity for the pure sand also increases from the onset of loading. The velocity increase is discontinuous, probably due to a misidentification of the shear arrival caused by high attenuation at low load. After the clay is added the decrease in shear velocity over the entire load range is more gradual than the increase for the sand.

The plots of Figure 6 show the variation of velocities for different clay contents in sand-clay mixtures at low and high loading stress. The velocities are not simple functions of added second phase. When data from the pure sand sample are used as a reference, it is apparent that the first addition of clay to sand increases the compressional velocity, suggesting that the clay acts as an adhesive. This increase persists at high stress. The shear velocity is less sensitive to the first addition of clay and decreases slightly, although the amplitude increases (Figure 2). Compressional velocity decreases when the clay content is increased to 10%, although this effect is reduced by additional stress. The shear velocity reaches a maximum at 10% clay concentration, and additional stress does not suppress the behavior.

Three waveforms plotted at the same scale (zero gauge units, 7.8 and 15.6 psi) for the 10% clay-sand sample are shown in Figure 7 to illustrate the effect of pressure. Both the compressional and shear arrivals are faster, with increasing load. The compressional amplitude increases only slightly, if at all. The shear amplitude increases with increasing load and also becomes sharper, consistent with a decrease in shear attenuation and more efficient transmission of high frequencies.

Microscopic Imaging

Ultrasonic measurements of compressional and shear velocities in dilute sand-clay mixtures demonstrate that small amounts of added clay can dramatically alter wave propagation as discussed in the previous section. The salinity of pore fluid is known to control clay morphology (Sposito 1994). In order to determine the effect of microstructure and clay morphology on the elastic response, we devised an experiment to directly observe how sand, clay and pore fluid interact on the grain scale.

Microscopic Imaging Setup

An optical microscope was used to observe relative positions of sand and clay and changes in clay morphology as a function of the chemistry of the pore fluid (Figure 8). We used a pure silica Ottawa sand with grain sizes between 74-420 microns and a median diameter (d_{50}) of 273 microns, mixed with 1, 3, and 10 weight-% of sodium montmorillonite, a swelling clay. The wetting fluids were deionized water and a 0.1 N $CaCl_2$ solution. The sand, clay and fluids were the same as those used in the ultrasonic experiments.

Results of Microscopic Observations

For the dry sand-clay mixture, we observed that the clay particles electrostatically cling to the sand grains but do not form a coating. Instead, in the dry mixture clay particles tended to bridge the gaps between grains, influencing how stresses are carried across grain contacts. As expected, when de-ionized water was added to this mixture, due to the chemical interactions between the clay and the water, the clay particles swelled to occupy the available pore space between sand grains. Subsequently, when wetted with $CaCl_2$, the clay particles settled and clumped

together to form larger clusters or flocs by a process called flocculation (Sposito, 1984).

Interpretation of Micrographs

The flocculation process depends mainly on the charge that may be present on the particles in solution. The charge on each particle may repel the other particles and keep the material in suspension, or it may cause the particles to be attracted to each other and form clusters (or flocs). Visual observations confirm that clays in the contact areas between quartz grains can have a large effect on elastic response even in dilute concentrations. These visual observations provide needed insight for analysis of laboratory ultrasonic velocity data using effective medium theories that have appropriate microstructural assumptions (e.g., Berge et al. 1999).

Discussion

The velocities observed for the sand-clay mixtures in this study are low, comparable or slightly higher than the velocity of air. The compressional velocities are lower than typical field values as compiled by Bourbié et al. (1987) and are slightly higher than values for near-surface sand reported by Bachrach et al. (1998). The admixed second phase can alter seismic attributes even for low mass fractions. The photomicrograph of sand-10% clay spread on a glass slide shown in Figure 8 suggests that the micromechanics of the small clay particles may explain this strong influence. The clay particles adhere electrostatically to the quartz grains with their long axes perpendicular to the surface and tend to bridge the gaps between quartz grains. The large increase in compressional velocity when clay is first added to sand accompanied by a decrease in shear attenuation suggests that the clay alters the grain contacts by acting as an adhesive. The clay mixture shows a decreasing velocity after the initial increase. It appears that at this stage the soft second phase disrupts the structure of the sand framework causing a decrease in velocity. As the mass fraction of the second phase continues to increase, porosity reduction dominates, generally producing the highest velocities. Finally, when the free porosity is eliminated, velocities begin to drop as the slow second phase becomes the framework. This behavior is similar to that reported by Marion et al. (1992), for sand/kaolinite mixtures at high pressures.

Acknowledgements

We thank B. Viani for advice on the selection of smectites. This work was performed under the auspices of the U.S. Department of Energy by the Lawrence Livermore National Laboratory under contract number W-7405-ENG-48 and supported specifically by the Environmental Management Science Program of the Office of Environmental Management and the Office of Energy Research.

References

Aki, K., and Richards,P. G., 1980, Quantitative Seismology, Theory and Methods, Vols. I and II, W. H. Freeman and Company, San Francisco, CA.

Aracne-Ruddle, C., D. Wildenschild, B. Bonner, and P. Berge, 1998, Direct observation of morphology of sand-clay mixtures with implications for mechanical properties in sediments (abstract): LLNL report UCRL-JC-131702 Abs, Eos, Transactions of the American Geophysical Union, 79, Fall Meeting Supplement, F820.

Bachrach, R., J. Dvorkin, and A. Nur, High-resolution shallow-seismic experiments in sand, Part II: Velocities in shallow unconsolidated sand, Geophysics, 63, 1233-1240, 1998.

Berge, P.A., J.G. Berryman, J.J. Roberts, and D. Wildenschild, 1998, Joint inversion of geophysical data for site characterization and restoration monitoring, EMSP project summary/progress report for FY98 for EMSP project 55411: LLNL report UCRL-JC-128343, presented at the DOE Environmental Management Science Workshop held July 27-July 30, 1998, Chicago, IL, sponsored by the DOE EMSP and the American Chemical Society.

Berge, P.A., J.G. Berryman, B.P. Bonner, J.J. Roberts, and D. Wildenschild, 1999, Comparing geophysical measurements to theoretical estimates for soil mixtures at low pressures: LLNL report UCRL-JC-132893, in Powers, M.H., L. Cramer, and R.S. Bell, Eds., Proceedings of the Symposium on the Application of Geophysics to Engineering and Environmental Problems (SAGEEP), March 14-18, 1999, Oakland, CA, Environmental and Engineering Geophysical Society, Wheat Ridge, CO, 465-472.

Bonner, B.P., D.J. Hart, P.A. Berge, and C.M. Aracne, 1997, Influence of chemistry on physical properties: Ultrasonic velocities in mixtures of sand and swelling clay (abstract): LLNL report UCRL-JC-128306abs, Eos, Transactions of the American Geophysical Union, 78, Fall Meeting Supplement, F679.

Bonner, B. P., Boro, C., and Hart, D. J., 1999, Anti-waveguide for ultrasonic testing of granular media under elevated stress, LLNL patent disclosure, in process, 1999.

Bourbié T., O. Coussy, and B. Zinszner, 1987, Acoustics of Porous Media, Gulf Pub. Co., Houston.

Domenico, S. N., 1976, Effect of brine-gas mixture on velocity in an unconsolidated sand reservoir: Geophysics 41, 882-894.

Hamilton, Edwin L., and Richard T. Bachman, 1982, Sound velocity and related properties of marine sediments, J. Acoust. Soc. Am., 72 (6), 1891-1904.

Harris, J. M., R. C. Nolen-Hoeksema, R. T. Langan, M. Van Schaack, S. K. Lazaratos, and J. W. Rector III, 1995, High-resolution crosswell imaging of a west Texas carbonate reservoir: Part 1--Project summary and interpretation: Geophysics 60, 667--681.

Trombino, C. N., 1998, Elastic properties of sand-peat moss mixtures from ultrasonic measurements: LLNL report UCRL-JC-131770, LLNL, Livermore, CA.

Lama, R.D., and V. S. Vutukuri, 1978, Handbook on Mechanical Properties of Rocks: Testing Techniques and Results, Volume II,
Trans tech Publications, Clausthal, Germany, 195-196.

Marion, D., A. Nur, H. Yin, and D. Han, Compressional velocity and porosity in sand-clay mixtures, Geophysics, 57, p 554-563, 1992.

Sears, F. M., and Bonner, B. P., 1981, Ultrasonic attenuation measurement by spectral ratios utilizing signal processing techniques: IEEE Trans. On Geoscience and Remote Sensing GE-19 , 95-99, 1981.

Sposito, G., 1984, The Surface Chemistry of Soils, Oxford University Press, New York & Clarendon Press, Oxford.
Steeples, D.W., Shallow seismic reflection section-- Introduction, Geophysics, 63, 1210-1213, 1998.
Whitman, Robert V., The response of soils to dynamic loadings, report no. 25: miscellaneous studies of the formation of wave fronts in sand, MIT Dept. of Civil Engineering Research Report R66-32, Soils Pub. No. 196, MIT, 1966.
Wyllie, M. R. J., A. R. Gregory, and G. H. F. Gardner, 1958, An experimental investigation of factors affecting elastic wave velocities in porous media: Geophysics, 23, 459-493.

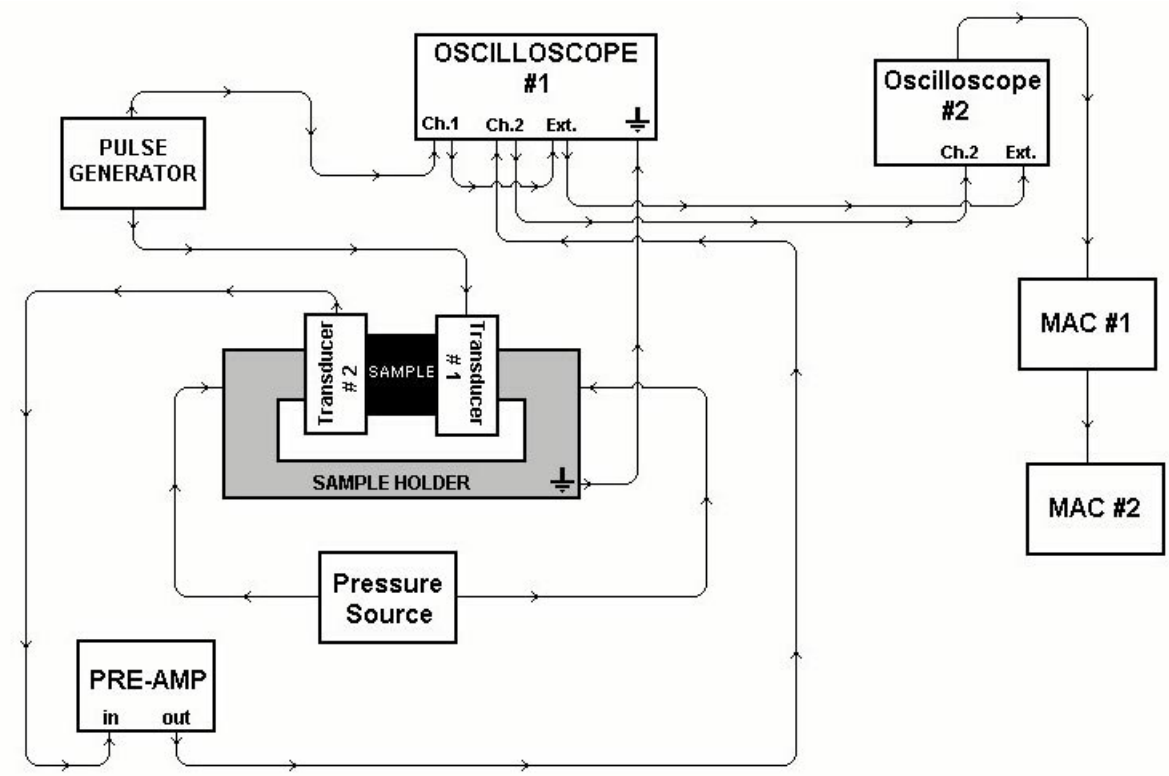

Figure 1. Schematic of the ultrasonic pulse transmission system, including the assembly for applying uniaxial load.

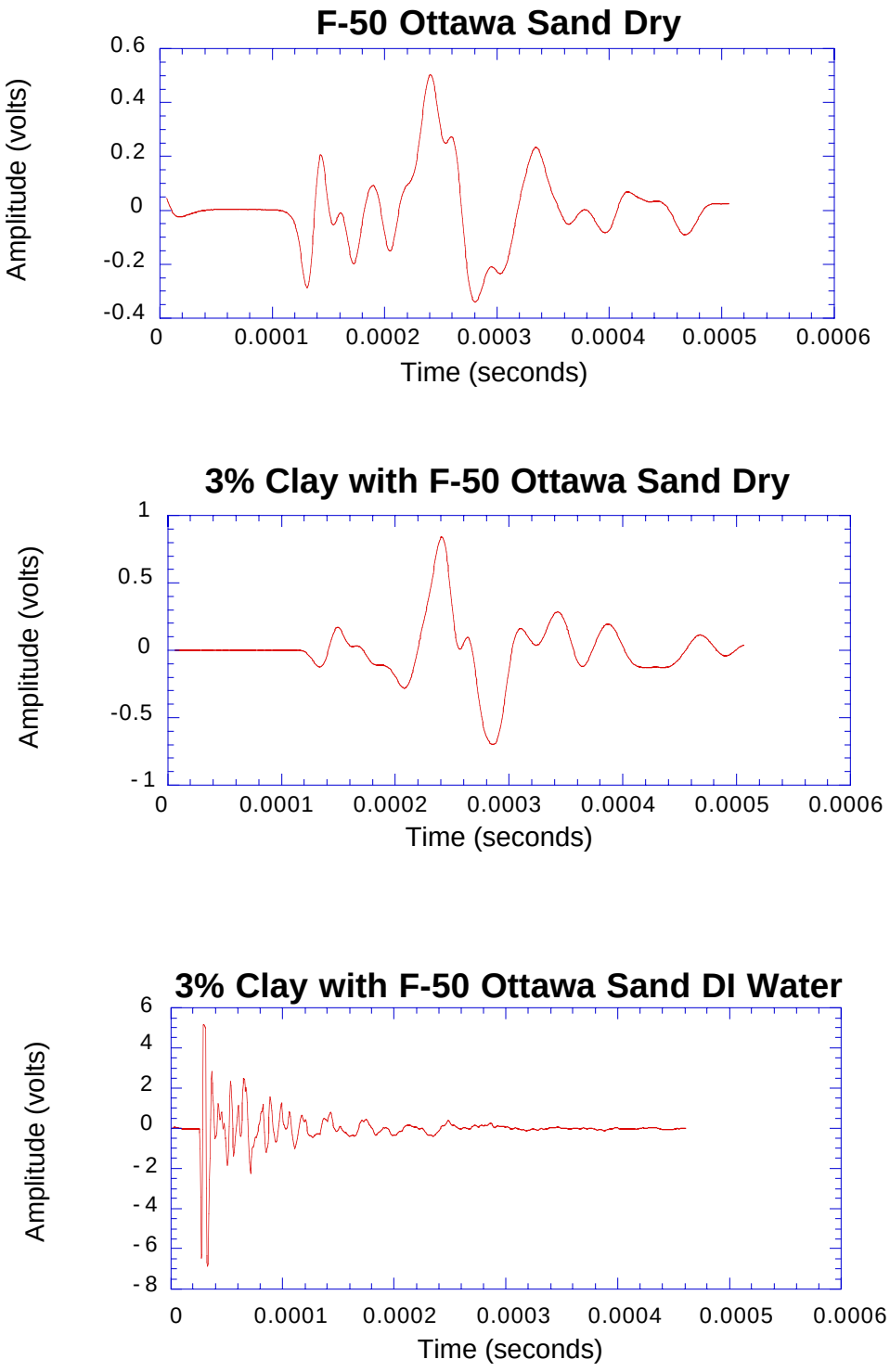

Figure 2. Received ultrasonic pulses for top:) dry sand; middle:) three percent clay-sand dry; and bottom:) three percent clay-sand saturated with de-ionized water.

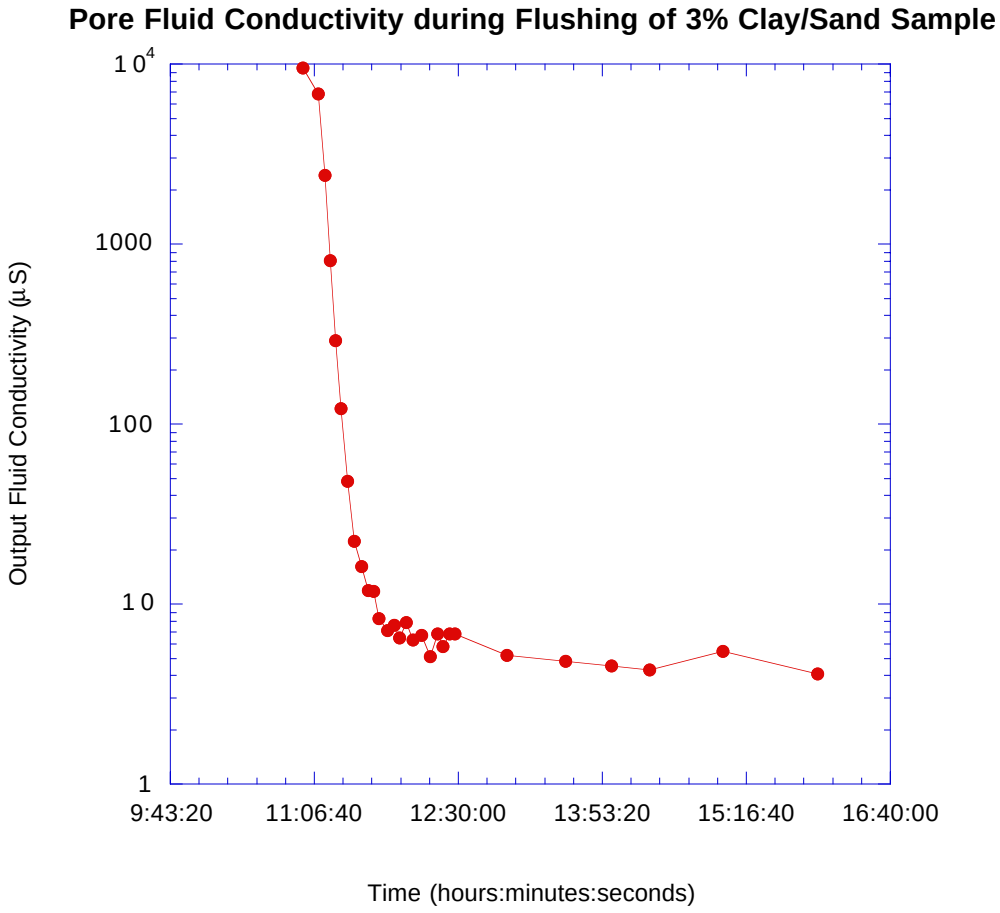

Figure 3a. Electrical conductivity of effluent during flushing of $CaCl_2$ saturated sample with DI water.

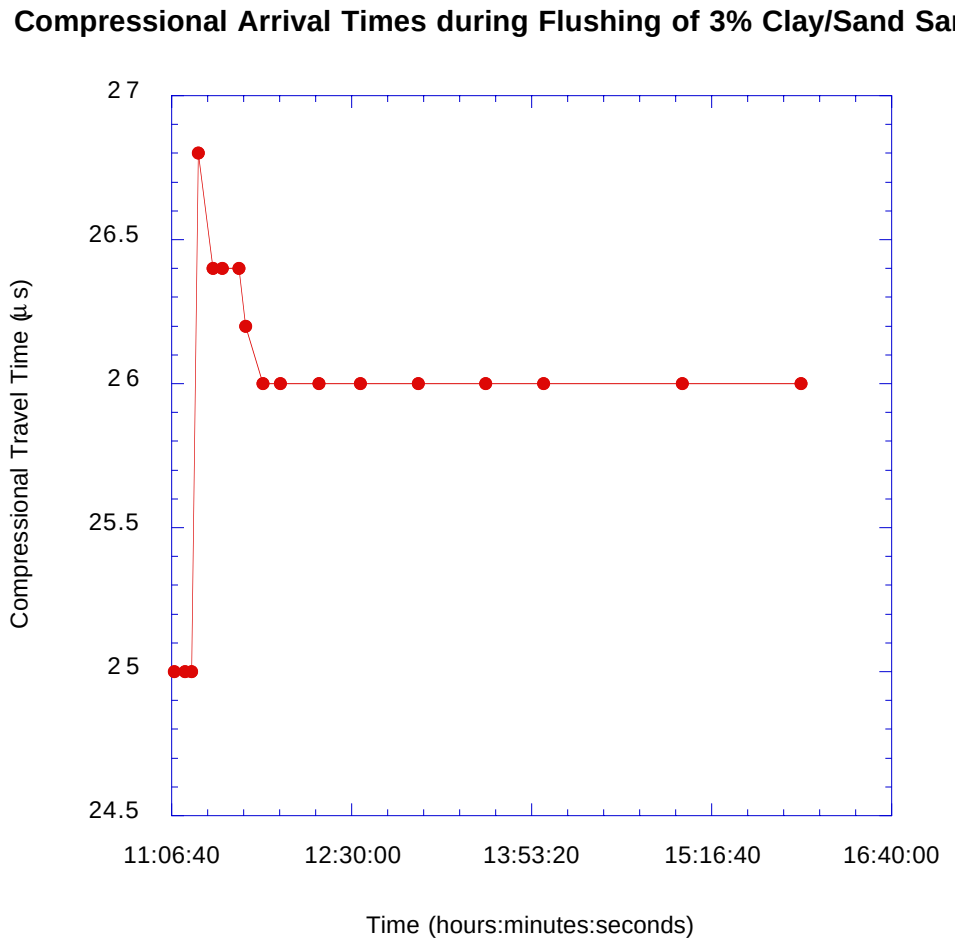

Figure 3b. Arrival times of compressional waves during flushing of $CaCl_2$ saturated sample with DI water.

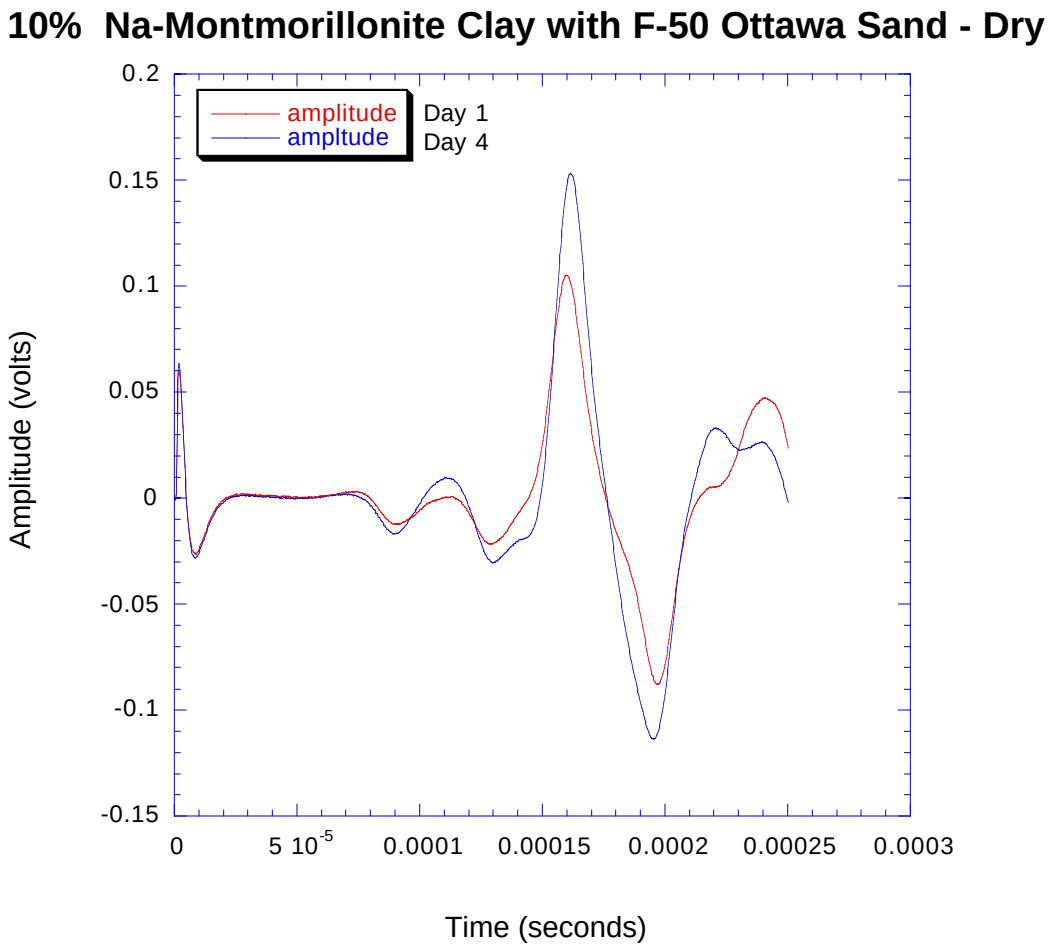

Figure 4. Waveforms for the 10% clay sample without load. The second waveform was collected after an interval of 4 days.

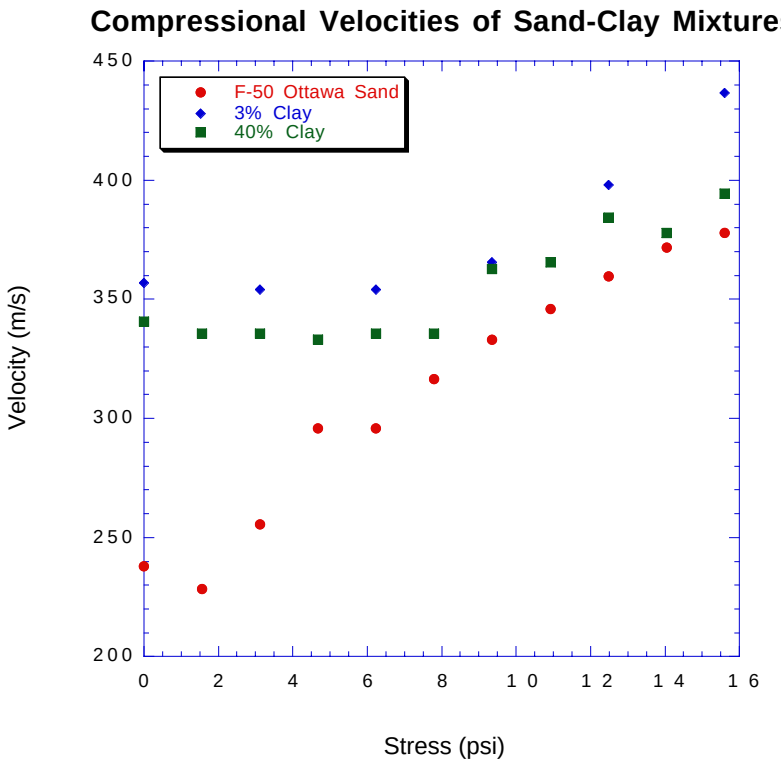

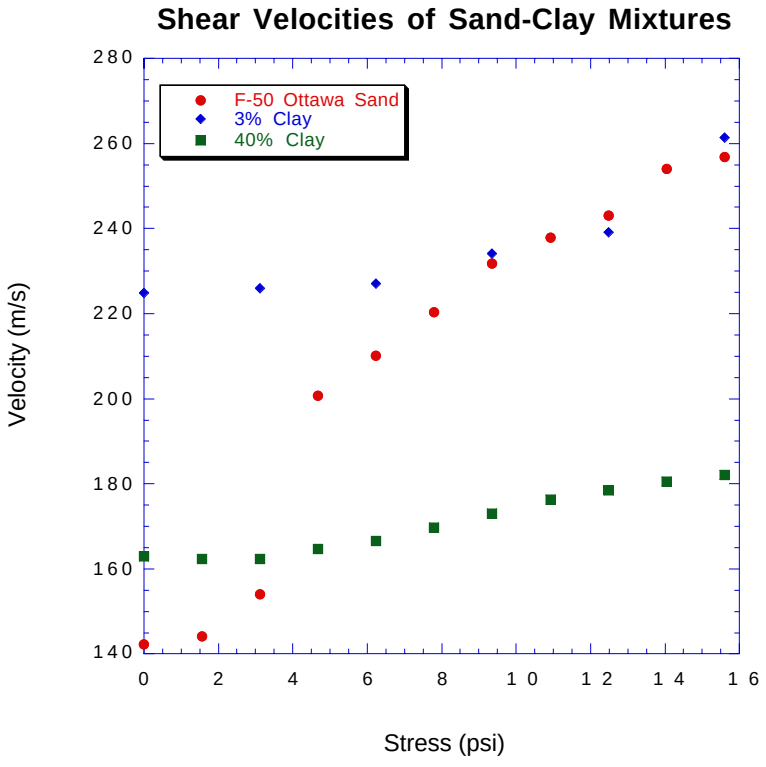

Figure 5. Uniaxial stress dependence of compressional and shear velocities for representative sand-clay mixtures.

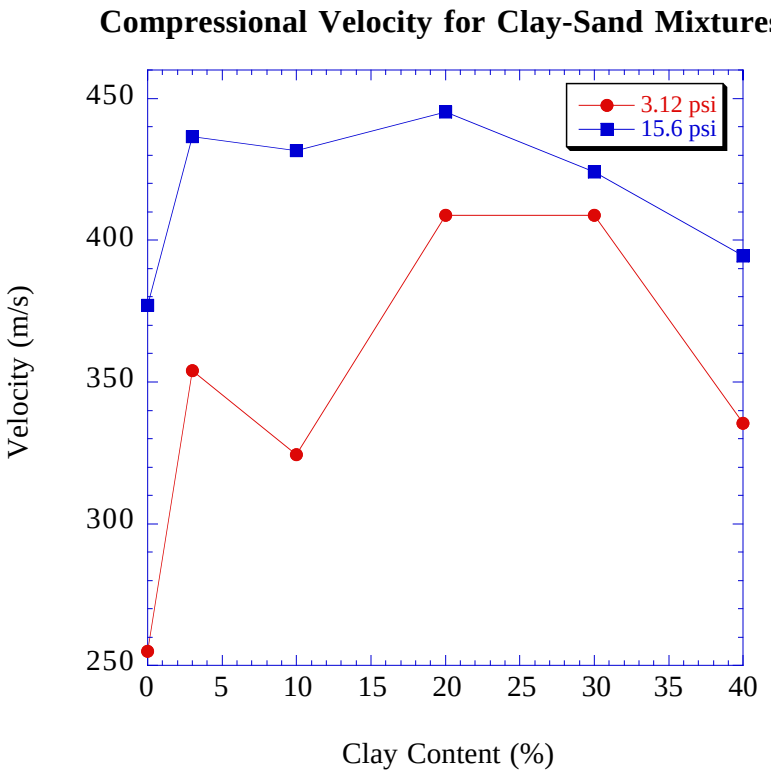

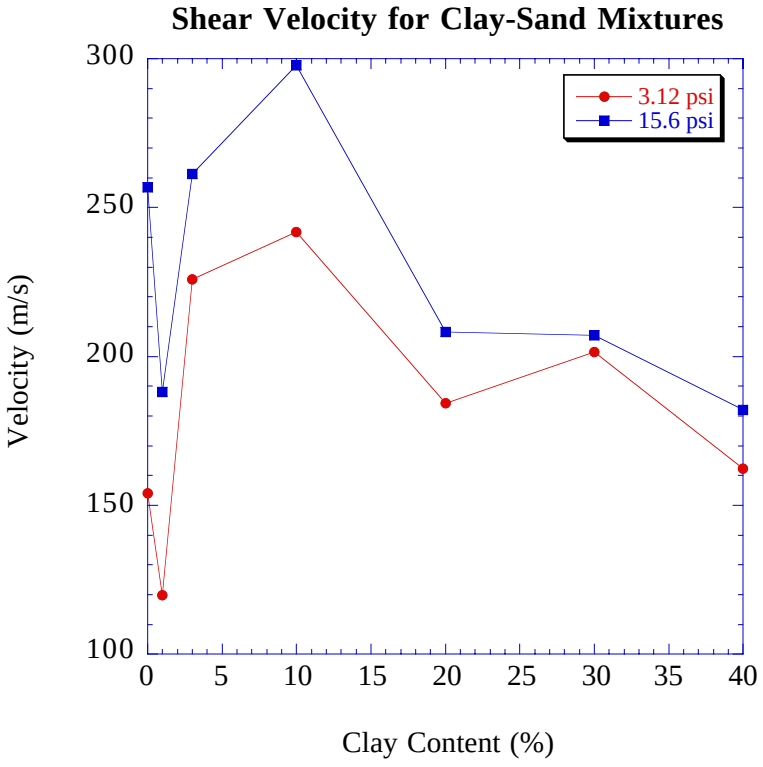

Figure 6. Ultrasonic velocities for two different loads as a function of added second phase.

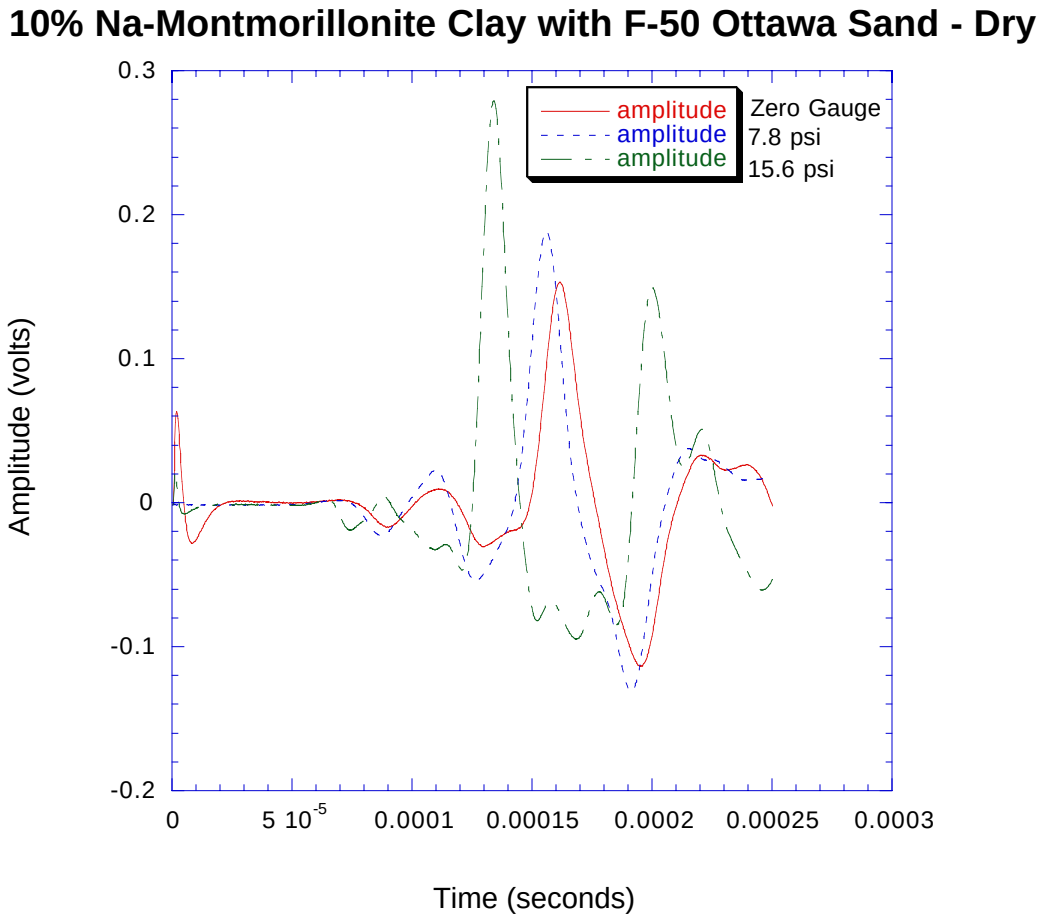

Figure 7. Waveforms for 10% clay-sand sample for three different load values.

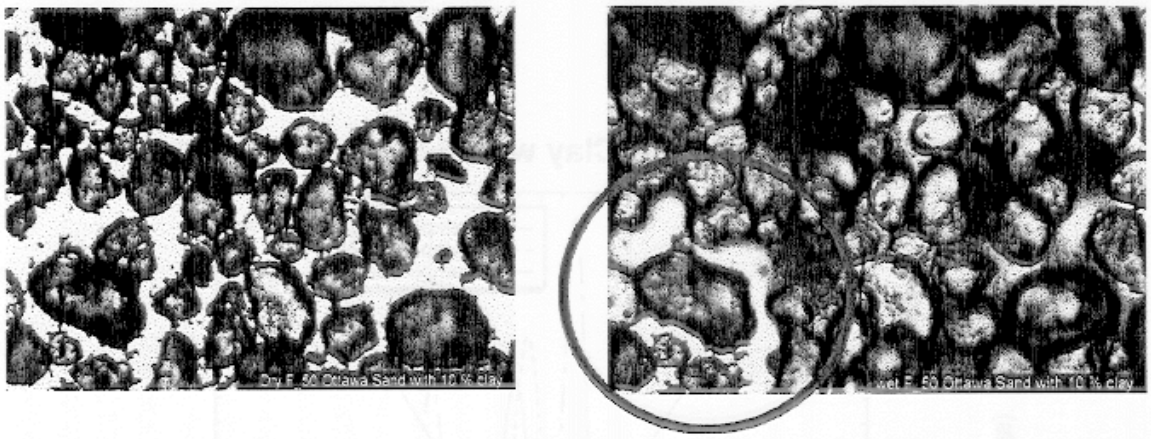

Figure 8. Photomicrographs of sand with ten percent clay. The grain size of the sand ranged from 74-420 microns with a mean of 273. The mixture in the left photograph is dry. The right photograph shows fluid advancing into the mixture. The circled area shows the boundary between fluid and gas phases.

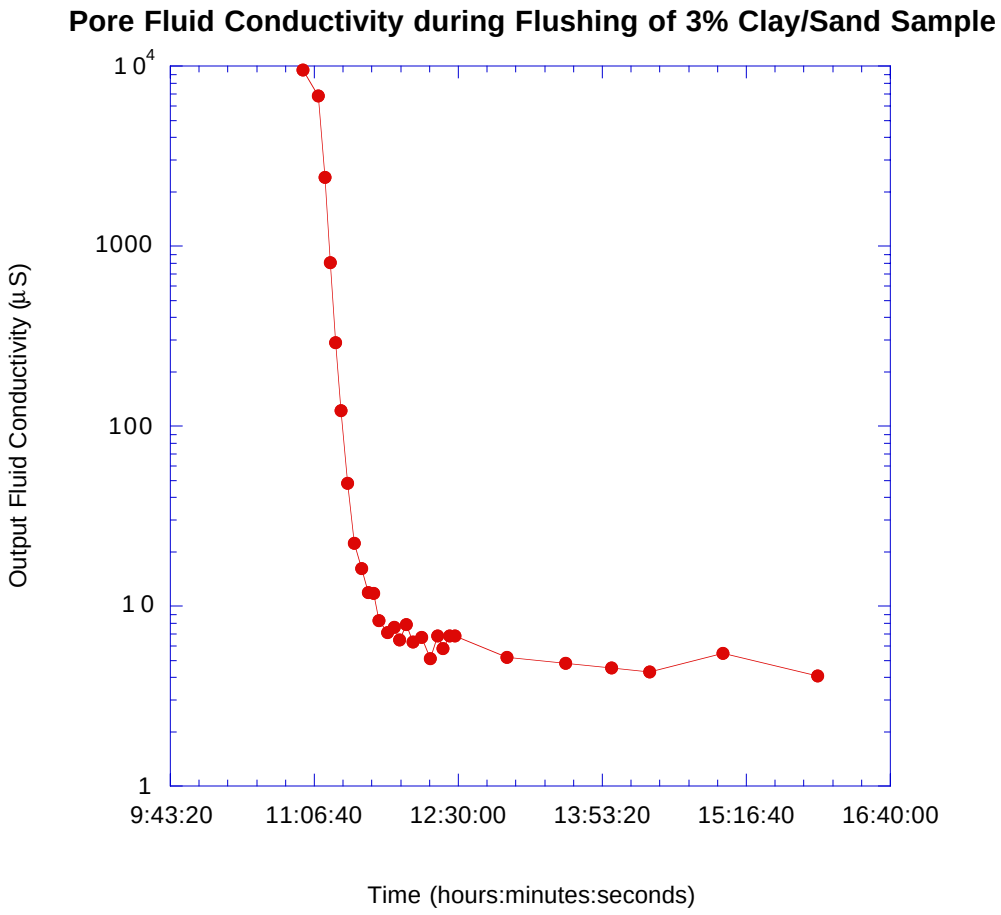

Figure 9. Pore fluid conductivity of 3% clay/sand sample during flushing with DI water.

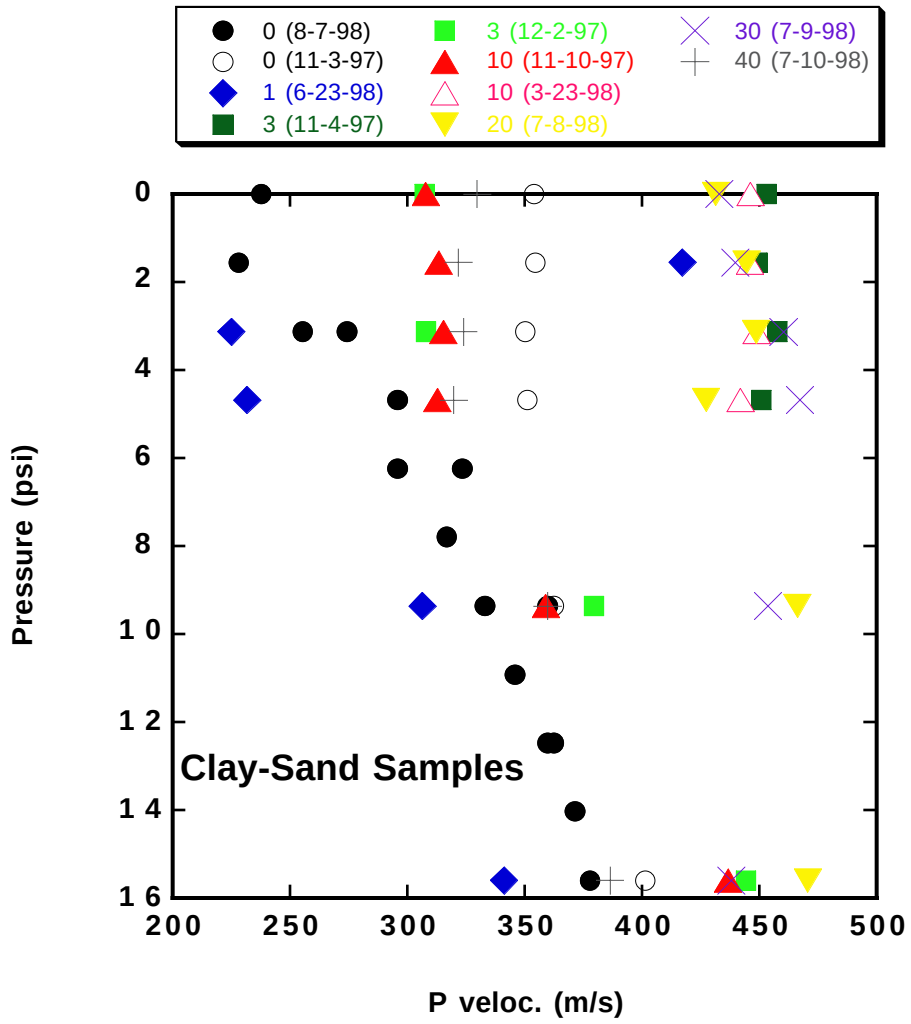

Figure 10. Compressional wave velocities for sand-clay layers (layers #1 and #3) in the sand-clay samples, from Table 5. See Appendix for details.

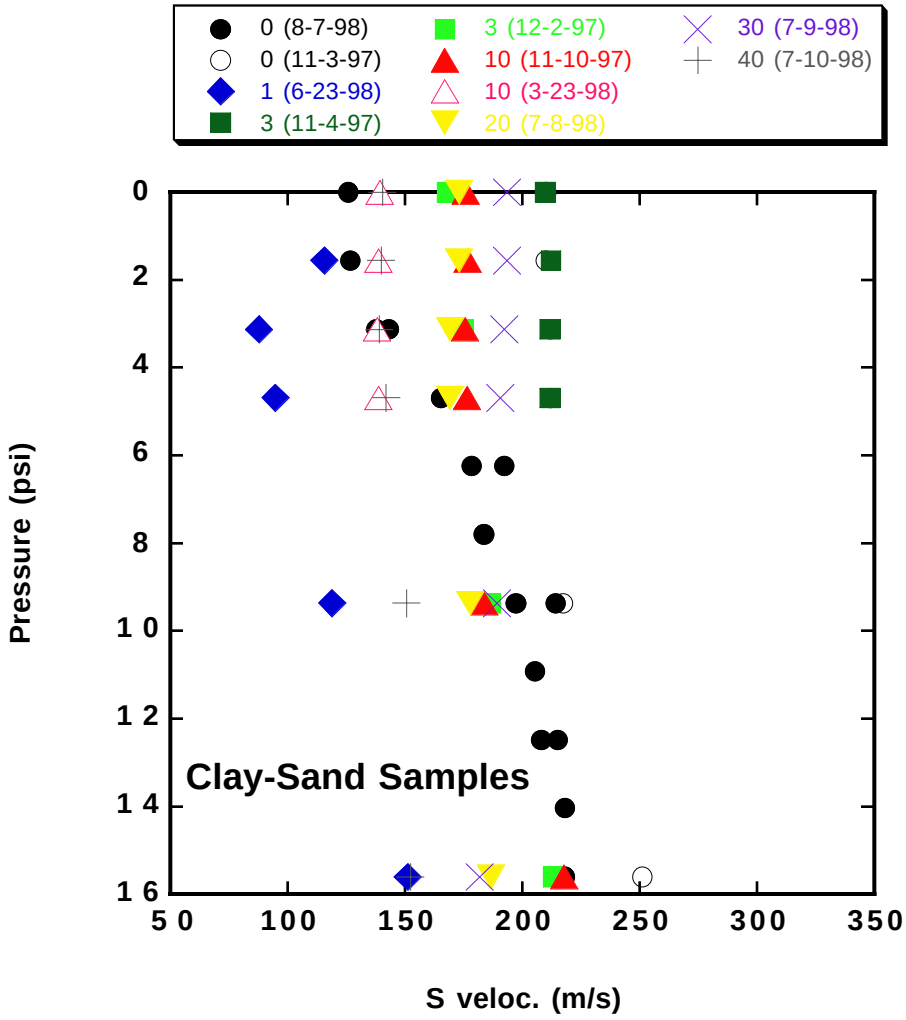

Figure 11. Shear wave velocities for sand-clay layers (layers #1 and #3) in the sand-clay samples, from Table 5. See Appendix for details.

APPENDIX

The sample densities presented in Table 1 and the velocities presented in Table 3 give the averages of these properties for each three-layers sample. With the exception of the pure sand sample, all other samples were built with a central layer of pure sand sandwiched between two sand-clay layers. In order to find the densities and velocities of the sand-clay layers, we have removed the effects of the middle sand layer to obtain the sand-clay densities presented in Table 4 and the sand-clay velocities presented in Table 5 and Figures 10 and 11. This appendix describes the procedures used to find these sand-clay properties.

Density Corrections

The densities of the sand-clay layers in each sample were found using the sample compositions and densities given in Table 1. The masses of the sand and clay used to construct the sand-clay layers (second and third columns of Table 1) were used to find the mass percentage of clay in the sand-clay layers for each sample (third column of Table 4). The masses of the middle sand layers for all the samples are given in Table 1 (7th column) and again in Table 4 (fourth column). The ratio of the mass of a middle sand layer compared to the mass of the sand in the pure sand sample provides an estimate of the volume of that sand layer, which in turn gives the relative volume of that pure sand layer with respect to the whole sample having a known volume of 78 cm^3. Differences in packing of the sand in the pure sand sample and the sand layers produce some uncertainty in these relative volume estimates, but this uncertainty is not expected to be significant and probably does not exceed the 5% uncertainty in the known volume of the sample holder. Table 4 gives the relative volumes of the middle sand layers in all the samples (fifth column). The individual layer masses for the sand-clay layers given in Table 1 (sixth and eighth columns) were combined to give the total mass of sand and clay making up the two sand-clay layers in each sample (Table 4, sixth column). (We assume that for any given sample, the two sand-clay layers have the same composition, but they may have different thicknesses.) The total sand-clay volume for the two sand-clay layers in each sample was found (Table 4, seventh column) by using the total volume of the sample holder and removing the volume of the pure sand layer using the information about relative volume of the sand. Finally, the sand-clay mass was divided by the sand-clay volume, for each sample, to obtain the density of the sand-clay mixture making up the two sand-clay layers in each sample (Table 4, eighth column). These density values have uncertainties of about 5%, because of the uncertainty in the total volume of the sample holder.

Velocity Corrections

The velocity correction procedure accounts for the traveltime through the pure sand layer in a three-layer sample by assuming that the velocity in that layer is the same as the velocity in the pure sand sample. Again, differences in packing of the sand may produce uncertainties in the estimated sand-clay properties, particularly for the measurements at the lowest pressures (about 0 to 6 psi) where the packing may have a significant effect on velocities. We used the traveltimes for the pure sand sample from 11-3-97 (Table 2) for the corrections, since the velocities measured as a function of pressure in that sample had small gradients and thus indicated that it was tightly packed. Therefore use of those data for corrections would not introduce negative gradient artifacts in the sand-clay velocity estimates. We estimate that velocity uncertainties for the sand-clay layers may be up to about 20 percent at the lowest pressures and about 10 percent at higher pressures, due to the combination of uncertainties in the pure sand velocities and packing effects.

For any given sand-clay sample, at a particular pressure, the traveltime in the sand layer is subtracted from the total traveltime through the sample, leaving the traveltime for the signal through the two sand-clay layers in the sample. The total traveltime is simply the value listed in Table 2. The traveltime in the sand layer is obtained by multiplying the traveltime in the pure sand sample (also given in Table 2) by the relative volume of the pure sand layer in the sample (from Table 4). (Note that the relative volume of the sand layer is proportional to the relative thickness of the layer for the nearly-cylindrical sample.) The uncertainty in the relative volume is about 5% as noted above. The t_0 system correction of 1 to 3 μs is insignificant compared to uncertainties related to volume and sand packing, and therefore we did not use the system correction when estimating the velocities for the sand-clay layers. Table 5 lists the measured traveltimes and measurement uncertainties for each sample, and the traveltimes for P and S signals through the pure sand layer of each sample.

The velocity at a given pressure for the sand-clay layers in a given sample is found by multiplying the traveltime through the sand-clay layers by the path length of the signal that travelled through the combined thicknesses of the two sand-clay layers. This path length can be found simply by using the known total length of the sample holder and subtracting the thickness of the middle sand layer, which is known from the relative volume of the sand layer as described above. Table 5 presents these velocity estimates for the sand-clay layers at various pressures. The compressional wave velocities for the sand-clay layers are shown in Figure 10, and Figure 11 presents the shear wave velocities.

After obtaining the estimates of velocities in the sand-clay layers presented in Table 5, we used the densities of the sand-clay layers given in Table 4 to estimate the bulk modulus and shear modulus of the sand-clay layers in each sample (see Eq. 1 and Eq. 2). These moduli estimates are given in Table 5. Moduli uncertainties are large, possibly 20 to 50%, because of the combined uncertainties in all the parameters used to calculate the moduli. The moduli estimates, however, provide useful information about the mechanical behavior of these unconsolidated sediments. The shear moduli are much smaller than the bulk moduli, as expected for unconsolidated materials, and both bulk and shear moduli are at least 3 orders of magnitude smaller than values typically found for sedimentary rocks.

The plots of the sand-clay velocities (Figures 10 and 11) show that the compressional wave velocities are about twice as large as the shear wave velocities for most sand-clay mixtures. Compressional wave velocities show steep gradients for one of the pure sand samples that may be loosely packed, and for the 1% sand-clay mixture. One of the 3% and one of the 10% sand-clay mixtures have steep velocity gradients at pressures above approximately 3 to 5 psi, and no gradient at lower pressures. This behavior may be due to differences in packing for these samples compared to the pure sand sample that was used to make the velocity corrections. The other sand-clay mixures do not show significant compressional velocity gradients. In general, the samples having higher clay contents have higher compressional wave velocities, but there is a lot of variation that may be due to packing rather than to clay content.

The shear wave velocities have small gradients and do not vary systematically with amount of clay. Humidity effects may explain some of the shear velocity behavior, and loose packing may produce the small shear velocity gradient observed for one of the pure sand samples.

TABLE 1														
					Mass (grams)			Density (kg/m^3)						
	Mixture			Sample										
Description	Clay (grams)	F-50 Sand (grams)	Total (grams)	Assembly (grams)	First Layer (Clay-Sand)	Second Layer (Sand)	Third Layer (Clay-Sand)	ρ_1	ρ_2	ρ_3	Total	Logbook page #	Date	Notes
Sand		131.97	161.61	29.64							1691.92	107	8/7/98	
1% Clay / 99% Sand	1.01	99.01	165.62	34.09	52.72	40.66	38.15	2027.69	1563.85	1467.31	1686.28	78	6/10/98	
3% Clay / 97% Sand			169.07	35.33	51.46	32.82	49.47	1979.23	1262.31	1902.69	1714.74	28	11/4/97	
3% Clay / 97% Sand			168.74	35.53	53.91	31.27	48.03	2073.46	1202.69	1847.31	1707.82	47	12/2/97	
3% Clay / 97% Sand	3	100.01	165.59	35.11	51.88	38.89	40.48	1995.38	1495.77	1556.92	1232.56	77	6/10/98	100% Humidity
10% Clay / 90% Sand			171.85	36.43	56.75	29.43	49.24	2182.69	1131.92	1893.85	1736.15	32	11/10/97	
10% Clay / 90% Sand			169.14	35.92	48.19	39.93	41.04	1853.46	1535.77	1578.46	1655.9	62	3/19/98	
10% Clay / 90% Sand			167.46	37.22	55.22	35.63	39.4	2123.85	1370.38	1515.38	1669.87	68	5/18/98	
10% Clay / 90% Sand	8.05	72.02	163.62	35.64	45.29	48.16	34.92	1741.92	1852.31	1343.08	1645.77	77	6/10/98	100% Humidity
20% Clay / 80% Sand	16.00	64.00	158.54	31.9	38.63	48.82	39.19	1485.77	1877.69	1507.31	1623.59	78	7/8/98	
30% Clay / 70% Sand	24	56	153.44	31.1	36.68	55.48	30.18	1410.77	2133.85	1160.77	1568.46	78	7/8/98	
40% Clay / 60% Sand	32.00	48.00	150.7	31.22	31.04	52.78	35.66	1193.85	2030	1371.54	1531.8	79	7/8/98	

Date	Sample Description	Pressure (gauge units)	Pressure (psi)	P arrival a (ms)	error (± ms)	P arrival b (ms)	error (± ms)	P arrival c (ms)	error (± ms)	S arrival a (ms)	error (± ms)	S arrival b (ms)	error (± ms)	S arrival c (ms)	error (± ms)	Saved as (time)
7-Aug-98	Dry F-50	0	0	190	10	237	5			319	7	360	3			951
Book # 1	Ottowa sand	5	1.56	198	10	239	5			315	8	358	5			1011
Page # 107		10	3.12	177	5	219	5			295	10	329	5			1018
		15	4.68	153	5	195	5			227	5	275	10			1024
		20	6.24	153	5	181	5			217	8	255	8			1028
		25	7.8	143	7	172	3			207	8	248	5	275	5	1033
		30	9.36	136	5	163	5			197	3	231	5	265	3	1038
		35	10.92	131	5	157	5			192	5	222	3	249	5	1043
		40	12.48	126	5	153	3			188	3	219	3			1048
		45	14.04	122	5	147	3			180	5	209	5			1053
		50	15.6	120	5	145	3			178	5	209	5			1057
		40	12.48	125	5	150	5			184	3	212	5			1104
		30	9.36	126	5	151	5			186	3	213	5			1108
		20	6.24	140	7	175	8			206	8	237	10			1113
		10	3.12	165	10	243	7			293	7	317	5			1120
		0	0	?		?				?		436	10			1130

Notes
saved 40db, used 60db to pick times 60db 40db   sank to 35 gauge sank to 15 gauge saved 40db, used 60db to pick times

TABLE 3a

8/7/98	Book #1	Page # 107		WAVE VELOCITIES F-50 SAND	
Clay:Sand	Pressure (MPa)	Pressure (psi)	Wave Type	Adjusted Arrival Time (μs)	Wave Velocity (m/s)
O:100	0.00000	0	P	189	237.9
			S	316	142.3
	0.01076	1.56	P	197	228.2
			S	312	144.1
	0.02153	3.12	P	176	255.5
			S	292	154.0
	0.03229	4.68	P	152	295.8
			S	224	200.7
	0.04306	6.24	P	152	295.8
			S	214	210.1
	0.05382	7.8	P	142	316.6
			S	204	220.4
	0.06458	9.36	P	135	333.0
ρ			S	194	231.8
1691.92	0.07535	10.92	P	130	345.8
			S	189	237.9
	0.08611	12.48	P	125	359.7
			S	185	243.0
	0.09688	14.04	P	121	371.6
			S	177	254.0
	0.10764	15.6	P	119	377.8
			S	175	256.9
	0.08611	12.48	P	122	368.5
			S	181	248.4
	0.06458	9.36	P	125	359.7
			S	183	245.7
	0.04306	6.24	P	139	323.5
			S	203	221.5
	0.02153	3.12	P	164	274.1
			S	290	155.0
	0.00000	0	P	?	
			S	?	

TABLE 3b

6/23/98 Clay:Sand	Book #2 Pressure (MPa)	Page # 71 Pressure (psi)	Wave Type	WAVE VELOCITIES 1% Adjusted Arrival Time (μs)	Wave Velocity (m/s)
1:99	0.01076	1.56	P	113	397.9
			S	297	151.4
	0.02153	3.12	P	177	254.0
			S	375	119.9
	0.03229	4.68	P	173	259.9
			S	333	135.0
	0.04306	6.24	P	161	279.3
			S	327	137.5
	0.04885	7.08	P	149	301.7
			S	289	155.6
	0.06458	9.36	P	139	323.5
			S	279	161.1
	0.07535	10.92	P	137	328.2
ρ			S	277	162.3
1686.28	0.08611	12.48	P	133	338.0
			S	265	169.7
	0.09688	14.04	P	123	365.5
			S	243	185.0
	0.10764	15.60	P	125	359.7
			S	239	188.1
	0.10764	15.60	P	93	483.4
			S	241	186.6
	0.09688	14.04	P	125	359.7
			S	249	180.6
	0.08611	12.48	P	125	359.7
			S	247	182.0
	0.07535	10.92	P	111	405.0
			S	255	176.3
	0.06458	9.36	P	133	338.0
			S	263	171.0
	0.04885	7.08	P	137	328.2
			S	273	164.7
	0.04306	6.24	P	137	328.2
			S	273	164.7

	0.03229	4.68	P	137	328.2
			S	271	165.9
	0.02153	3.12	P	157	286.4
			S	269	167.1
	0.01076	1.56	P	137	328.2
			S	269	167.1

Note: Molasses used as coupling agent

TABLE 3c

11/6/97 Book # 1 Page # 31 WAVE VELOCITIES 3%

Clay:Sand	Pressure (MPa)	Pressure (psi)	Wave Type	Adjusted Arrival Time (μs)	Wave Velocity (m/s)
3:97	0.00000	0	P	126	356.8
			S	200	224.8
	0.02153	3.12	P	127	354.0
			S	199	225.9
	0.04306	6.24	P	127	354.0
			S	198	227.1
ρ	0.06458	9.36	P	123	365.5
			S	192	234.2
9/10/08	0.08611	12.48	P	113	397.9
			S	179	251.2
	0.10764	15.6	P	103	436.5
			S	172	261.4

TABLE 3d

11/10/97 Book #1 Page #32 WAVE VELOCITIES 10%

Clay:Sand	Pressure (MPa)	Pressure (psi)	Wave Type	Adjusted Arrival Time (μs)	Wave Velocity (m/s)
10:90	0.00000	0	P	141	318.9
			S	187	240.4

	0.01076	1.56	P	139	323.5
			S	186	241.7
	0.02153	3.12	P	138.6	324.4
			S	186	241.7
	0.03229	4.68	P	139.4	322.5
			S	185	243.0
	0.04306	6.24	P	139	323.5
			S	182	247.0
	0.05382	7.8	P	124.2	362.0
			S	177	254.0
	0.06458	9.36	P	124.2	362.0
ρ			S	174	258.4
1736.15	0.07535	10.92	P	117	384.3
			S	171	262.9
	0.08611	12.48	P	113.4	396.5
			S	163	275.8
	0.09688	14.04	P	111	405.0
			S	158	284.6
	0.10764	15.6	P	104.2	431.5
			S	151	297.7
	0.08611	12.48	P	105.8	425.0
			S	154	291.9
	0.06458	9.36	P	121.8	369.1
			S	168	267.6
	0.04306	6.24	P		
			S	209	215.1
	0.0215	3.12	P		

	3				
			S	217	207.2

TABLE 3e

7/8/98 Book #1 Page # 79 WAVE VELOCITIES 20%

Clay:Sand	Pressure (MPa)	Pressure (psi)	Wave Type	Adjusted Arrival Time (μs)	Wave Velocity (m/s)
20:80	0.00000	0	P	112	401.4
			S	241	186.6
	0.01076	1.56	P	110	408.7
			S	241	186.6
	0.02153	3.12	P	110	408.7
			S	244	184.3
	0.03229	4.68	P	113	397.9
			S	244	184.3
	0.04306	6.24	P	112	401.4
			S	241	186.6
	0.05382	7.8	P	104	432.3
			S	240	187.3
	0.06458	9.36	P	106	424.2
ρ			S	234	192.1
1623.59	0.07535	10.92	P	105	428.2
			S	229	196.3
	0.08611	12.48	P	104	432.3
			S	224	200.7
	0.09688	14.04	P	103	436.5
			S	221	203.4

0.10764	15.6	P	101	445.1
		S	216	208.1
0.08611	12.48	P	102	440.8
		S	218	206.2
0.06458	9.36	P	104	432.3
		S	225	199.8
0.04306	6.24	P	115	391.0
		S	240	187.3
0.02153	3.12	P	121	371.6
		S	248	181.3
0.00000	0	P	116	387.6
		S	249	180.6

TABLE 3f

7/9/98 Book #1 Page # 82 WAVE VELOCITIES 30%

Clay:Sand	Pressure (MPa)	Pressure (psi)	Wave Type	Adjusted Arrival Time (μs)	Wave Velocity (m/s)
30:70	0.00000	0	P	113	397.9
			S	223	201.6
	0.01076	1.56	P	112	401.4
			S	223	201.6
	0.02153	3.12	P	110	408.7
			S	223	201.6
	0.03229	4.68	P	109	412.5
			S	224	200.7
	0.04306	6.24	P	113	397.9
			S	225	199.8
	0.05382	7.8	P	112	401.4
			S	225	199.8
	0.06458	9.36	P	109	412.5
ρ			S	223	201.6

1568.46	0.07535	10.92	P	108	416.3
			S	222	202.5
	0.08611	12.48	P	107	420.2
			S	221	203.4
	0.09688	14.04	P	107	420.2
			S	218	206.2
	0.10764	15.6	P	106	424.2
			S	217	207.2
	0.08611	12.48	P	107	420.2
			S	221	203.4
	0.06458	9.36	P	107	420.2
			S	221	203.4
	0.04306	6.24	P	111	405.0
			S	234	192.1
	0.02153	3.12	P	114	394.4
			S	233	193.0
	0.00000	0	P	111	405.0
			S	233	193.0

TABLE 3g

7/10/98 Book #1 Page # 85 WAVE VELOCITIES 40%

Clay:Sand	Pressue (MPa)	Pressure (psi)	Wave Type	Adjusted Arrival Time (μs)	Wave Velocity (m/s)
40:60	0.00000	0.00	P	132	340.6
			S	276	162.9
	0.01076	1.56	P	134	335.5
			S	277	162.3
	0.02153	3.12	P	134	335.5
			S	277	162.3
	0.03229	4.68	P	135	333.0
			S	273	164.7
	0.04306	6.24	P	134	335.5

			S	270	166.5
	0.05382	7.80	P	134	335.5
			S	265	169.7
	0.06458	9.36	P	124	362.6
ρ			S	260	172.9
1531.80	0.07535	10.92	P	123	365.5
			S	255	176.3
	0.08611	12.48	P	117	384.3
			S	252	178.4
	0.09688	14.04	P	119	377.8
			S	249	180.6
	0.10764	15.60	P	114	394.4
			S	247	182.0
	0.08611	12.48	P	116	387.6
			S	252	178.4
	0.06458	9.36	P	115	391.0
			S	256	175.6
	0.04306	6.24	P	122	368.5
			S	273	164.7
	0.02153	3.12	P	123	365.5
			S	275	163.5
	0.00000	0.00	P	213	211.1
				325	138.3

TABLE 4	Sand-Clay	Densities					
Description	Date	Mass Clay	Sand Layer (#2)	Sand Layer	Total (Layers #1+#3)	Total Sand-Clay	Sand-Clay
	Created	(%)	Mass (g)	Volume (%)	Sand-Clay Mass (g)	Volume (cc)	Density (g/cc)
Sand		0.00	131.97	100.00	0.00	78 (sand)	1.7 (pure sand)
1% Clay / 99% Sand	6/10/98	1.01	40.66	30.81	90.87	54	1.7
3% Clay / 97% Sand	11/4/97	3.00	32.82	24.87	100.93	59	1.7
3% Clay / 97% Sand	12/2/97	3.00	31.27	23.69	101.94	60	1.7
3% Clay / 97% Sand	6/10/98	2.91	38.89	29.47	92.36	55	1.7
10% Clay / 90% Sand	11/10/97	10.00	29.43	22.30	105.99	61	1.8
10% Clay / 90% Sand	3/19/98	10.00	39.93	30.26	89.23	54	1.6
10% Clay / 90% Sand	5/18/98	10.00	35.63	27.00	94.62	57	1.7
10% Clay / 90% Sand	6/10/98	10.05	48.16	36.49	80.21	50	1.6
20% Clay / 80% Sand	7/8/98	20.00	48.82	36.99	77.82	49	1.6
30% Clay / 70% Sand	7/8/98	30.00	55.48	42.04	66.86	45	1.5
40% Clay / 60% Sand	7/8/98	40.00	52.78	39.99	66.70	47	1.4

Notes
100% Humid.
100% Humid.

TABLE 5	Sand-Clay	Velocities	and Moduli
Pure Sand	11/3/97	p. 26	
Pressure	P traveltime (a)	P uncertainty	S traveltime (a)
(psi)	(μs)	(μs)	(μs)
0	128	5	217
1.56	128	5	217
3.12	129	5	215
4.68	129	5	215
9.36	125	4	210
15.6	113	4	182
Pure Sand	12/2/97	p. 47	
Pressure	P traveltime (a)	P uncertainty	S traveltime (mean a,b)
(psi)	(μs)	(μs)	(μs)
0	106	2	230
9.36	108	2	227
15.6	105	2	225
Pure Sand	8/7/98	p. 107	
Pressure	P traveltime (a)	P uncertainty	S traveltime (b)
(psi)	(μs)	(μs)	(μs)
0	190	10	360
1.56	198	10	358
3.12	177	5	329
4.68	153	5	275
6.24	153	5	255
7.8	143	7	248
9.36	136	5	231
10.9	131	5	222
12.5	126	5	219
14	122	5	209
15.6	120	5	209
12.5	125	5	212
9.36	126	5	213
6.24	140	7	237
3.12	165	10	317
1% Clay-Sand	6/23,24/1998	p. 71,73	
Pressure	P traveltime	P uncertainty	S traveltime
	Sample (pick a)		Sample (pick b)
(psi)	(μs)	(μs)	(μs)
1.56	114	32	336
3.12	178	34	420
4.68	174	30	394
9.36	140	28	326

15.6	126	12	262
3% Clay-Sand	**11/4/97**	**p. 28**	
Pressure	**P traveltime**	**P uncertainty**	**S traveltime**
	Sample (pick a)		**Sample (pick a)**
(psi)	**(μs)**	**(μs)**	**(μs)**
0	106	4	215
1.56	107	3	213
3.12	106	3	213
4.68	107	3	213
3% Clay-Sand	**11/6/97**	**p. 31**	
Pressure	**P traveltime**	**P uncertainty**	**S traveltime**
	Sample (pick a)		**Sample (pick b)**
(psi)	**(μs)**	**(μs)**	**(μs)**
0	127	4	238
3.12	128	4	241
9.36	124		231
15.6	104	13	212
3% Clay-Sand	**12/2/97**		
Pressure	**P traveltime**	**P uncertainty**	**S traveltime**
	Sample (pick a)		**Sample (mean of a&b)**
(psi)	**(μs)**	**(μs)**	**(μs)**
0	142	5	256
3.12	142	5	247
9.36	120	2	234
15.6	104		204
10% Clay-Sand	**11/10/97**	**p. 32**	
Pressure	**P traveltime**	**P uncertainty**	**S traveltime**
	Sample (pick a)		**Sample (mean of b&c)**
(psi)	**(μs)**	**(μs)**	**(μs)**
0	142	10	247
1.56	140	10	246
3.12	140	10	247
4.68	140	10	246
9.36	125	5	237
15.6	105	5	201
10% Clay-Sand	**3/23/98**	**p. 63**	
Pressure	**P traveltime**	**P uncertainty**	**S traveltime**
	Sample (pick a)		**Sample (pick b)**
(psi)	**(μs)**	**(μs)**	**(μs)**
0	109	2	291
1.56	109	2	292

3.12	109	2	292
4.68	110	38	291
20% Clay-Sand	**7/8/98**	**p. 79**	
Pressure	**P traveltime**	**P uncertainty**	**S traveltime**
	Sample (pick a)		**Sample (pick a)**
(psi)	**(μs)**	**(μs)**	**(μs)**
0	113	5	244
1.56	111	5	244
3.12	111	5	247
4.68	114	50	247
9.36	107	5	237
15.6	102	5	219
30% Clay-Sand	**7/9/98**	**p. 82**	
Pressure	**P traveltime**	**P uncertainty**	**S traveltime**
	Sample (pick a)		**Sample (pick a)**
(psi)	**(μs)**	**(μs)**	**(μs)**
0	114	5	226
1.56	113	5	226
3.12	111	5	226
4.68	110	5	227
9.36	110	5	226
15.6	107	5	220
40% Clay-Sand	**7/10/98**	**p. 85**	
Pressure	**P traveltime**	**P uncertainty**	**S traveltime**
	Sample (pick a)		**Sample (pick a)**
(psi)	**(μs)**	**(μs)**	**(μs)**
0	133	5	279
1.56	135	5	280
3.12	135	5	280
4.68	136	5	276
9.36	125	5	263
15.6	115	5	250

S uncertainty	**P velocity**	**S velocity**	**K**	**G**	
(μs)	**(m/s)**	**(m/s)**	**(MPa)**	**(MPa)**	
7	354	210	110	75	
8	355	210	110	75	
9	350	212	110	76	
10	351	212	110	76	
10	363	217	120	80	
6	401	251	130	110	
S uncertainty	**P velocity**	**S velocity**	**K**	**G**	
(μs)	**(m/s)**	**(m/s)**	**(MPa)**	**(MPa)**	
4	428	198	220	67	
3	420	201	210	68	
3	432	203	230	70	
S uncertainty	**P velocity**	**S velocity**	**K**	**G**	
(μs)	**(m/s)**	**(m/s)**	**(MPa)**	**(MPa)**	
3	238	126	60	27	
5	228	127	52	27	
5	255	138	68	32	
10	296	165	87	46	
8	296	178	77	54	
5	317	184	94	57	
5	333	197	100	66	
3	346	205	110	72	
3	360	208	120	74	
5	372	218	130	81	
5	378	218	140	81	
5	363	215	120	79	
5	360	214	120	78	
10	323	192	94	63	
5	274	143	81	35	
S uncertainty	**P traveltime**	**S traveltime**	**P velocity**	**S velocity**	**K**
	Pure Sand	**Pure Sand**	**Sand-Clay**	**Sand-Clay**	**Sand-Clay**
(μs)	**(μs)**	**(μs)**	**(m/s)**	**(m/s)**	**(MPa)**
36	128	217	417	116	270
44	129	215	225	87.9	69
58	129	215	232	94.9	71
44	125	210	307	119	130

20	113	182	341	151	150
S uncertainty	**P traveltime**	**S traveltime**	**P velocity**	**S velocity**	**K**
	Pure Sand	**Pure Sand**	**Sand-Clay**	**Sand-Clay**	**Sand-Clay**
(μs)	**(μs)**	**(μs)**	**(m/s)**	**(m/s)**	**(MPa)**
4	128	217	453	210	250
7	128	217	449	212	240
7	129	215	458	212	250
7	129	215	451	212	240
S uncertainty	**P traveltime**	**S traveltime**	**P velocity**	**S velocity**	**K**
	Pure Sand	**Pure Sand**	**Sand-Clay**	**Sand-Clay**	**Sand-Clay**
(μs)	**(μs)**	**(μs)**	**(m/s)**	**(m/s)**	**(MPa)**
35	128	217	355	184	140
39	129	215	352	180	140
36	125	210	364	189	140
37	113	182	445	203	240
S uncertainty	**P traveltime**	**S traveltime**	**P velocity**	**S velocity**	**K**
	Pure Sand	**Pure Sand**	**Sand-Clay**	**Sand-Clay**	**Sand-Clay**
(μs)	**(μs)**	**(μs)**	**(m/s)**	**(m/s)**	**(MPa)**
13	128	217	307	168	97
23	129	215	308	175	92
20	125	210	380	186	170
9	113	182	444	213	230
S uncertainty	**P traveltime**	**S traveltime**	**P velocity**	**S velocity**	**K**
	Pure Sand	**Pure Sand**	**Sand-Clay**	**Sand-Clay**	**Sand-Clay**
(μs)	**(μs)**	**(μs)**	**(m/s)**	**(m/s)**	**(MPa)**
18	128	217	308	176	96
18	128	217	313	177	100
20	129	215	315	175	110
20	129	215	313	176	100
20	125	210	359	184	150
40	113	182	437	218	230
S uncertainty	**P traveltime**	**S traveltime**	**P velocity**	**S velocity**	**K**
	Pure Sand	**Pure Sand**	**Sand-Clay**	**Sand-Clay**	**Sand-Clay**
(μs)	**(μs)**	**(μs)**	**(m/s)**	**(m/s)**	**(MPa)**
5	128	217	446	139	280
2	128	217	446	139	280

2	129	215	449	138	280
3	129	215	442	139	270
S uncertainty	**P traveltime**	**S traveltime**	**P velocity**	**S velocity**	**K**
	Pure Sand	**Pure Sand**	**Sand-Clay**	**Sand-Clay**	**Sand-Clay**
(μs)	**(μs)**	**(μs)**	**(m/s)**	**(m/s)**	**(MPa)**
5	128	217	432	173	230
5	128	217	445	173	250
5	129	215	449	169	260
5	129	215	427	169	230
5	125	210	466	178	280
5	113	182	471	187	280
S uncertainty	**P traveltime**	**S traveltime**	**P velocity**	**S velocity**	**K**
	Pure Sand	**Pure Sand**	**Sand-Clay**	**Sand-Clay**	**Sand-Clay**
(μs)	**(μs)**	**(μs)**	**(m/s)**	**(m/s)**	**(MPa)**
5	128	217	433	193	210
5	128	217	440	193	220
5	129	215	460	192	240
5	129	215	467	191	260
5	125	210	454	189	240
5	113	182	438	182	220
S uncertainty	**P traveltime**	**S traveltime**	**P velocity**	**S velocity**	**K**
	Pure Sand	**Pure Sand**	**Sand-Clay**	**Sand-Clay**	**Sand-Clay**
(μs)	**(μs)**	**(μs)**	**(m/s)**	**(m/s)**	**(MPa)**
3	128	217	330	140	120
3	128	217	322	140	110
3	129	215	324	139	110
3	129	215	320	142	110
3	125	210	360	151	140
3	113	182	386	152	170

G
Sand-Clay
(MPa)
23
13
15
24

39
G
Sand-Clay
(MPa)
75
77
76
76
G
Sand-Clay
(MPa)
57
55
61
70
G
Sand-Clay
(MPa)
48
52
59
77
G
Sand-Clay
(MPa)
56
56
55
56
61
85
G
Sand-Clay
(MPa)
31
31

31
31
G
Sand-Clay
(MPa)
48
48
46
46
51
56
G
Sand-Clay
(MPa)
56
56
55
55
54
49
G
Sand-Clay
(MPa)
28
27
27
28
32
32